The role of added mass in the dispersion of bubble clouds

IOP Conf. Series: Earth and Environmental Science **240** (2019) 062050 doi:10.1088/1755-1315/240/6/062050

The role of added mass in the dispersion of bubble clouds

S. Zoghlami[1], C. Béguin[1], S. Etienne[1], D. Scott[2], L. Bornard[2]

[1] Polytechnique Montréal, Mechanical Engineering Departement, Canada.
[2] Hydrodynamics Engineering, Hydro Solutions, GE Renewable Energy, Canada.

E-mail: stephane.etienne@polymtl.ca

Abstract. The mechanics of bubble clouds are essential to many industrial processes in the energy and chemical realms. In the specific case of hydroelectric turbines, bubble clouds are present when air is injected into the flow to increase dissolved oxygen content in the water flowing through the power plant. Modeling water flows through hydroelectric turbines already presents many difficulties; adding two-phase flows increases the complexity of the models. In particular, modeling the physics of the phenomena driving the mixing of bubbles in turbines is still a challenge. One important factor in existing two-phase flow models is modeling bubble dispersion. In two-phase flows, bubble dispersion comes from different sources such as turbulence, local pressure conditions and bubble-bubble interactions. In this study, we investigate the effect of added mass on the dispersion of bubbles. In the Euler-Lagrange modeling, the contribution of the added mass force in bubbly flow dispersion was quantified by the development of a repulsive force. This force is a consequence of the added mass variation. We called it the Meshchersky force. For the Euler-Euler model, the dispersion due to the added mass variation was not observed. In fact, the added mass coefficient used in this work was developed as a scalar. It was calculated in the acceleration direction. Thus, the resulting Meshchersky force has the same direction as the velocity. A better modeling would consider the added mass as a tensor rather than a scalar. Therefore, taking into account the void fraction gradient dependency to develop a correlation for the added mass tensor would be a solution to adequately model the added mass and Meshchersky forces, and hence bubble dispersion.

1. Introduction

The dispersion of bubbly flows is one of several challenges not resolved yet in two-phase flow modeling. This phenomenon can be produced from different mechanisms like turbulence, local pressure conditions and bubble-bubble interactions. The added mass fluctuation resulting from the motion of the surrounding bubbles is one of the paths to investigate in the comprehension of bubble dispersion. A first glimpse of the mechanisms at play comes from the study of two bubbles rising side-by-side in a stagnant column of water. The effects of added mass and induced added mass drive bubbles away from each other. As underlined by Milne-Thomson [1], the fact that added mass increases as bubbles come closer to each other creates a repelling force. Actually, the added mass corresponds to the kinetic energy in the liquid due to bubble motion. Consequently, if a bubble is moving towards another bubble without extraneous forces, the total energy must remain constant. Since its added mass increases, its velocity must decrease. The bubble is therefore repelled from other bubbles. This phenomenon minimizes the occurrence of impact between bubbles and contributes to the dispersion of bubble clouds. Biesheuvel and Wijngaarden [2], analytically resolved the potential flow around two rigid particles immersed in a perfect liquid and implicitly quantified the divergence of bubbles due to added mass.

Although it is not the sole mechanism that leads to the dispersion of bubbles, the role of added mass has not been adequately quantified and it is often not taken into account in classical bubbly two-phase flow

models. This study aims at assessing the effect of added mass in the dispersion of various bubble clouds. In particular, void fraction spreading will be compared between numerical methods and experimental results. The analytical solution of the potential flow and the added mass coefficient, previously developed in our group (see [3]), are used to model the bubble-bubble interaction. These models were used to develop a numerical model with Matlab that simulates a bubble cloud with the Euler-Lagrange approach. We created user-defined routines inside a commercial software solution (CFX 19) for the Euler-Euler approach. Two sets of experiments are used for comparison. The first data comes from experiments inside a bubble column of 15 cm by 15 cm [4]. The second one reproduces experiments inside a rectangular flume of 25 m $\times$ 1.2 m $\times$ 0.8 m in which air is injected through a circular nozzle of 6 mm diameter [5].

Our main goal is to develop a numerical strategy to simulate adequately bubbly two-phase flows. Both Euler-Euler and Euler-Lagrange approaches are used in order to include added mass and induced added mass models and to discuss their capacity to represent mechanical interactions between bubbles. The Euler-Lagrange model is based on discrete evolution of particles (bubbles or drops) inside a continuous liquid phase. The equation of motion for all bubbles should be resolved taking into account all the bubble-bubble interactions. If all mechanisms are well presented this model has a high accuracy. However, it is expensive from the point of view of numerical effort. Thus, it is usually used for bubbly flows with low void fractions. The Euler-Euler model considers both phases as continuous media. Its formulation is based on the averaging process of the local and instantaneous mass and momentum conservation equations. This model needs less numerical effort and can be used for industrial scales. However, the averaging process leads to a loss of information that should be adequately modeled and included as closure relations.

The tensors of added mass and induced added mass coefficients used in this work for the Euler-Lagrange approach lead to a good representation of the repelling force resulting from the added mass variation. This effect was not captured with the Euler-Euler model. Since the added mass coefficient, developed for the Euler-Euler model, are actually scalars, the resulting force from the added mass variation is produced in the velocity direction and has no transverse effect on the flow. Thus, no significant influence was observed on the dispersion phenomenon. Considering the added mass as a tensor rather than a scalar would give a better modeling for the dispersion mechanism with the Euler-Euler model. Therefore, taking into account the void fraction gradient dependency to develop a correlation for the added mass tensor would be a solution to adequately model the added mass and bubble dispersion.

2. Euler-Lagrange modeling

The Euler-Lagrange model is also known as the particle tracking model. In this modeling, bubbles are followed individually and all interactions are representative of the local arrangement of bubbles. This makes this approach more rich in terms of bubble to bubble interactions than the Euler-Euler approach. To track the bubble motion, we resolve the bubble motion equation considering only the drag force and the added mass as external forces acting on the bubble. In doing so, the quality of the results will only depend on the accuracy of the drag and the added mass modeling.

2.1. Added mass force

In what follows, we detail how we model the added mass force for the Euler-Lagrange approach. We assume that a potential flow approximation suffices to determine the added mass force [2, 6]. Thus, considering the flow incompressible, liquid velocity $\vec{U}_\ell$ around N_b bubbles derives from a potential Φ. Since the velocity must satisfy the mass conservation equation, the flow potential should be a solution for the Laplace equation. Due to the linearity of the Laplace equation, the velocity potential can be expressed as :

$$\Phi = \sum_{n=1}^{N_b} \sum_{j=1}^{3} \varphi_{nj} \dot{x}_{nj} \tag{1}$$

$j = 1, 2, 3$ refer respectively to the spatial directions x, y, z and $\dot{x}_{nj}$ to the velocity component of bubble n in the j direction. φ_{nj} is the potential flow that ensures the non-penetration on all the N_b bubbles and fulfills the following condition:

$$\dot{x}_{kj} = \delta_{kn}\delta_{ij} \times 1[m/s] \quad \forall i \in [1,3]\,,\ \forall k \in [1, N_b] \tag{2}$$

with δ_{kn} and δ_{ij} Kronecker symbols.
Pressure P is retrieved using the unsteady Bernoulli's formula :

$$P = -\rho_\ell \frac{D\Phi}{Dt} - \frac{1}{2}\rho_\ell \vec{U}^2 + \rho_\ell \nabla\Phi \cdot \vec{U} - \rho_\ell g z \tag{3}$$

with ρ_ℓ the liquid phase density, g the gravity and z the displacement in the gravity direction. The total force acting on the bubble k, based on the potential flow, is the integral of the pressure on its boundary. Thus, the added mass force is deduced from the time derivative of the flow potential :

$$\vec{F}_k = -\rho_\ell \int_{\theta=0}^{\pi}\int_{\varphi=0}^{2\pi} \frac{D\Phi}{Dt} d\vec{S}_k \tag{4}$$

$$= \underbrace{-\rho_\ell \int_{\theta=0}^{\pi}\int_{\varphi=0}^{2\pi} \sum_{n=1}^{N_b}\sum_{j=1}^{3} \varphi_{nj}\ddot{x}_{nj} d\vec{S}_k}_{\vec{F}_{M_k}} \underbrace{-\rho_\ell \int_{\theta=0}^{\pi}\int_{\varphi=0}^{2\pi} \sum_{n=1}^{N_b}\sum_{j=1}^{3} \frac{D\varphi_{nj}}{Dt}\dot{x}_{nj} d\vec{S}_k}_{\vec{F}_{Me_k}} \tag{5}$$

The added mass force acting on bubble k is the sum of two components $\vec{F}_{M_k}$ and $\vec{F}_{Me_k}$.
$\vec{F}_{M_k}$ contains two components; the added mass proportional to k^{th} bubble acceleration and the induced added mass proportional to all the other bubbles acceleration :

$$\vec{F}_{M_k} = \underbrace{\rho_\ell \int_{\theta=0}^{\pi}\int_{\varphi=0}^{2\pi} \varphi_{kj}\ddot{x}_{kj} d\vec{S}_k}_{\text{added mass}} + \underbrace{\rho_\ell \int_{\theta=0}^{\pi}\int_{\varphi=0}^{2\pi} \sum_{\substack{n=1\\ n\neq k}}^{N_b}\sum_{j=1}^{3} \varphi_{nj}\ddot{x}_{nj} d\vec{S}_k}_{\text{induced added mass}} \tag{6}$$

$$\vec{F}_{M_k} = -\rho_\ell \frac{4\pi a_k^3}{3} \sum_{n=1}^{N_b} \bar{\bar{\mathbf{C}}}_{nk} \ddot{\vec{x}}_n \tag{7}$$

The tensor of the added mass coefficients $\bar{\bar{\mathbf{C}}}_{nk}$ has been determined in Beguin et al. [3] as a function of the location of the surrounding bubbles $\vec{x}_{kn}$:

$$\bar{\bar{\mathbf{C}}}_{nk} = -\frac{3}{4\pi a_k^3} \int_{\theta=0}^{\pi}\int_{\varphi=0}^{2\pi} \begin{Bmatrix} \varphi_{n1} \\ \varphi_{n2} \\ \varphi_{n3} \end{Bmatrix} \otimes d\vec{S}_k \tag{8}$$

As φ_{nj} depend on the location of bubbles, we have $\vec{F}_{Me_k}$:

$$\vec{F}_{Me_k} = \rho_\ell \int_{\theta=0}^{\pi}\int_{\varphi=0}^{2\pi} \sum_{n=1}^{N_b}\sum_{j=1}^{3} \frac{D\varphi_{nj}}{Dt}\dot{x}_{nj} d\vec{S}_k \tag{9}$$

$$\vec{F}_{Me_k} = \underbrace{-\rho_\ell \frac{4\pi a_k^3}{3} \left(\sum_{n=1}^{N_b}\sum_{j=1}^{3} \frac{D\bar{\bar{\mathbf{C}}}_{kk}}{Dx_{nj}}\dot{x}_{nj} \right) \dot{\vec{x}}_k}_{\text{Meshchersky force}} \underbrace{-\rho_\ell \frac{4\pi a_k^3}{3} \sum_{\substack{n=1\\ n\neq k}}^{N_b}\sum_{j=1}^{3} \left(\frac{D\bar{\bar{\mathbf{C}}}_{nk}}{Dx_{kj}}\dot{x}_{kj} + \frac{D\bar{\bar{\mathbf{C}}}_{nk}}{Dx_{nj}}\dot{x}_{nj} \right) \dot{\vec{x}}_n}_{\text{induced Meshchersky force}} \tag{10}$$

We denoted the second component of the added mass force as a Meshchersky force since it is induced by the varying added mass due to the surrounding bubbles. As discussed previously, based on the energy analysis, this force should have a repelling effect on approaching bubbles.

2.2. Drag force

Since we are using spherical rigid bubbles at this stage of our work and considering Reynolds numbers under 500, we opted for the Schiller [7] drag coefficient given as :

$$C_D = \frac{24}{Re}\left(1 + 0.15Re^{0.687}\right) \tag{11}$$

This correlation was initially developed for a spherical rigid bubble with $Re < 800$ and in [8] it was proven that its applicability holds for $Re < 3 \times 10^5$. For the sake of validation, we compared the coefficient values given by the Schiller (1933) model to high quality experimental data carefully selected by [9] from several published papers. It is shown in **Figure 1.** that this correlation gives a good description of the experimental data.

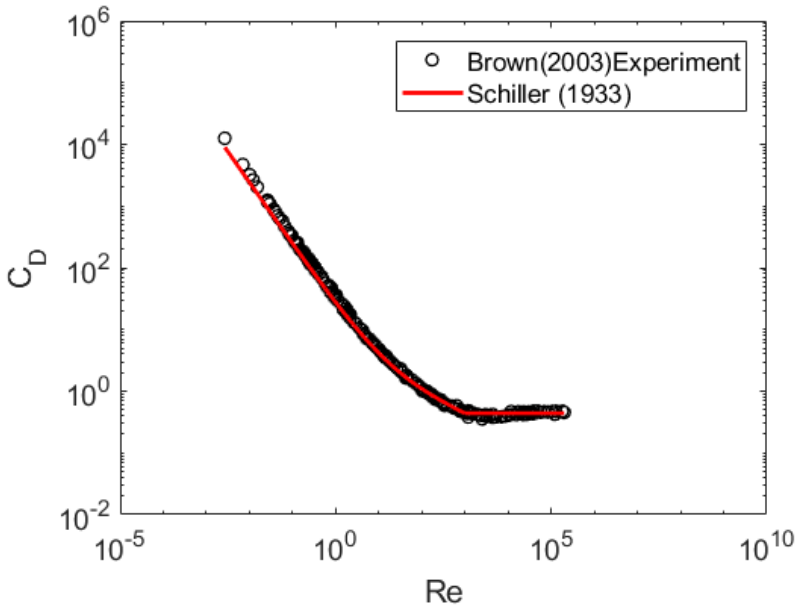

Figure 1: Schiller [7] drag coefficient validation.

2.3. Numerical approach

A Matlab implementation of the time evolution of several bubble groups has been developed. Forces acting on each bubble result from interactions between the bubbles, drag and buoyancy. We consider small groups of bubbles on which we demonstrate the effectiveness of the Meshchersky part of the added mass force at dispersing bubbles.

First configurations are 2D arrangements of N bubbles (2, 5, 9), with $2mm$ diameter, horizontally aligned with different pitches of 2.25 mm and 2.5 mm and no initial velocity. The time history of the horizontal displacement of the rightmost bubble of each configuration is shown in **Figure 2.**. We observe that the distribution of those bubble arrangements were expanded by more than 25% over the first 5 s which corresponds to an increase in area by more than 50%. We also observed that the displacement of the rightmost bubble depends on the number of bubbles aligned and on the pitch between the bubbles. Second configurations are 3D arrangement of N bubbles (27, 125) in a cuboid configuration. Bubbles are equally spaced by 2.5 mm and 2.25 mm in the x and y axis and 5 mm in the z direction. As shown in **Figure 3.**, over 2 s, the bubble cloud volume increased by over 55%. **Figure 4.** shows the effect of increasing the number of bubbles and initial gap between bubbles on the lateral time displacement of a bubble at the extreme edge of various arrangements. It can be concluded that the more bubbles there are in a configuration and the closer they initially are, the more important is the expansion.

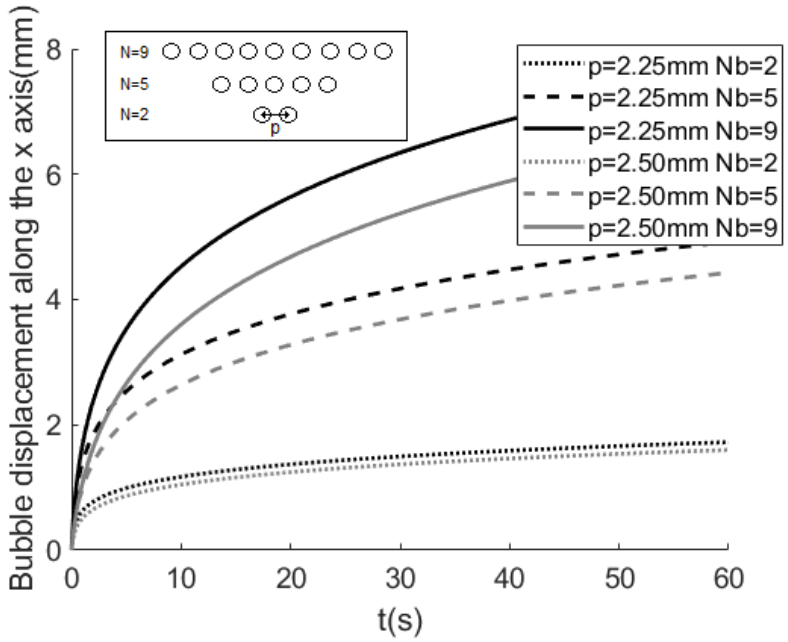

Figure 2: History of the horizontal displacement of the rightmost bubble for various 2D bubble arrangements.

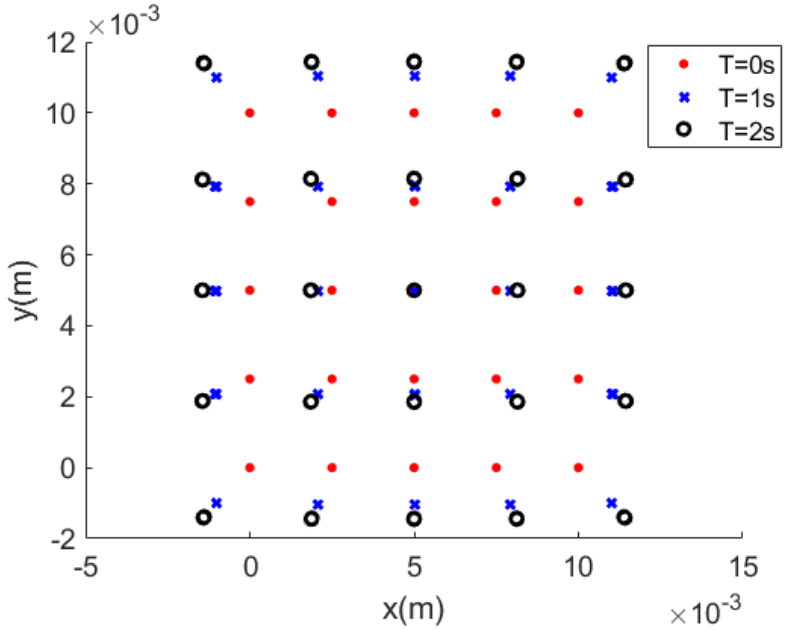

Figure 3: 3D bubble cloud configuration with 125 bubbles at t=0s, t=1s and t=2s seen from above.

3. Euler-Euler modeling

The Euler-Euler approach, also known as the two-fluid model, describes both the continuous and the dispersed phases as interpenetrating continua in an Eulerian framework. Its formulation is based on the averaging process of the local and instantaneous mass and momentum conservation equations for each phase and by incorporating the concept of phasic volume fraction ε_k. For an isothermal two phase flow,

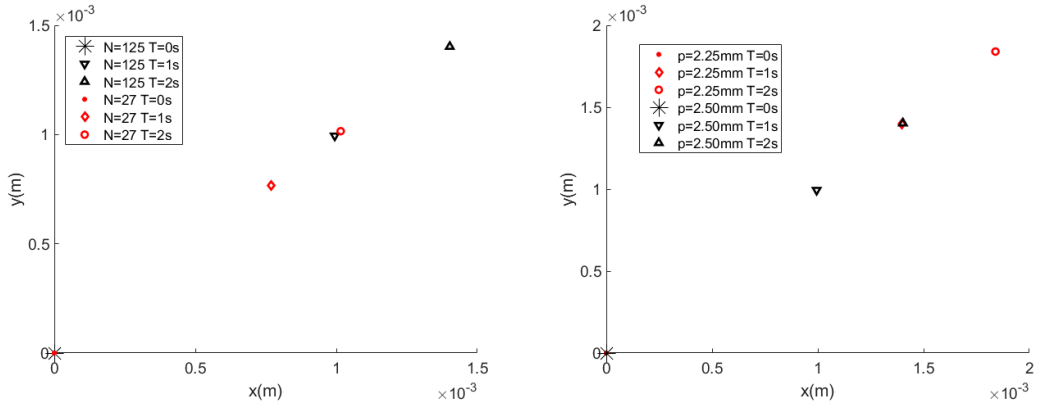

Figure 4: Displacement of a bubble at the extreme edge at t=0s, t=1s and t=2s for (left) two 3D arrangements of 27 and 125 bubbles and 2.5mm pitch and (right) arrangements of 125 bubbles with two different pitches of 2.5mm and 2.25mm.

the space averaged conservation equations (mass and momentum) for both phases ($k = \ell$ or g) reads :

$$\begin{aligned} \frac{\partial}{\partial t}\left(\varepsilon_k \rho_k\right) + \nabla \cdot \left(\varepsilon_k \rho_k \vec{U}_k\right) &= \Gamma_k \\ \frac{\partial}{\partial t}\left(\varepsilon_k \rho_k \vec{U}_k\right) + \nabla \cdot \left(\varepsilon_k \rho_k \vec{U}_k \otimes \vec{U}_k\right) &= -\varepsilon_k \nabla P_k + \varepsilon_k \rho_k \vec{g} + \nabla \cdot \left(\varepsilon_k \bar{\bar{\tau}}_k\right) + \vec{M}_k^i \end{aligned} \tag{12}$$

Γ_k is the mass fluxes through the interface. Mass conservation makes that the loss of mass from one phase is gained by the other which translates to:

$$\Gamma_\ell + \Gamma_g = 0 \tag{13}$$

$\vec{M}_k^i$ represents the momentum exchange between both phases through the interface. By neglecting the surface tension, the momentum exchange imposes that :

$$\vec{M}_\ell^i + \vec{M}_g^i = \vec{0} \tag{14}$$

The unknowns of the resulting system of equations are :

- 6 scalars : the void fraction ε which is ε_g (by definition $\varepsilon_\ell = 1 - \varepsilon_g$), pressures P_g, P_ℓ, densities ρ_g, ρ_ℓ and mass transfer between both media Γ_g, Γ_ℓ.
- 4 vectors : Velocities $\vec{U}_g$, $\vec{U}_\ell$ and momentum transfers between both media $\vec{M}_g^i$, $\vec{M}_\ell^i$.
- 2 tensors : stress tensors $\bar{\bar{\tau}}_g$, $\bar{\bar{\tau}}_\ell$

This amounts to 12 unknowns (scalars, vectors and tensor) whereas only 6 equations (3 scalar, 3 vector) are available. We need 3 scalar, 2 vector and 2 tensor equations to close the system.
To resolve the system some assumptions were adopted for the numerical solution :

- No mass transfer between the phases ($\Gamma_\ell = \Gamma_g = 0$).
- Dynamic equilibrium between the two phases ($P_\ell = P_g = P$).
- Incompressible fluids : ρ_g and ρ_ℓ are constant.
- $\varepsilon_k \left(\bar{\bar{\tau}}_k + \bar{\bar{\tau}}_k^{Re}\right) = \varepsilon_k \mu_k \left[\nabla \vec{U}_k + \left(\nabla \vec{U}_k\right)^T\right]$ with $\mu_k = \mu_{k_{mol}} + \mu_{k_{turb}}$
- The interface momentum exchange is defined by the sum of various forces acting on both phases $\vec{M}_\ell^i = -\vec{M}_g^i = \sum \vec{f}$

Since we aim to evaluate the added mass force effect on the flow dynamics, the momentum transfer for the present study contains only drag and added mass forces. Lift, two-phase flow turbulence and law of the wall forces are thus ignored. They shall require a modeling in the future once proper models have been developed. The turbulence viscosity stemming from Boussinesq assumption is also set to zero. In fact, for bubbles there is no turbulence because the flow is of Stokes kind. In the continuous phase, not enough knowledge is available to define turbulence when void fraction is higher than a few per cent (See Lance and Bataille [10]). These assumptions allow the definition of the 7 supplementary unknowns and to close the system of equations.
In the numerical model, assuming incompressible flows in both media, volume conservation reads:

$$\sum_k \frac{1}{\rho_k}\left[\frac{\partial}{\partial t}\left(\varepsilon_k\rho_k\right)+\nabla\cdot\left(\varepsilon_k\rho_k\vec{U}_k\right)\right]=0 \tag{15}$$

$$\sum_k \varepsilon_k = 1 \Rightarrow \sum_k \nabla\cdot\left(\varepsilon_k\vec{U}_k\right)=0 \tag{16}$$

Interface forces resume to:

$$\vec{M}_\ell^i = -\vec{M}_g^i = \vec{f}_{M\ell}+\vec{f}_{D\ell} \tag{17}$$

The drag is defined as

$$\vec{f}_{D_\ell} = \frac{3}{4}\varepsilon_g\rho_\ell\frac{C_D}{d_b}\left\|\vec{U}_g-\vec{U}_\ell\right\|\left(\vec{U}_g-\vec{U}_\ell\right) \tag{18}$$

and added mass, is implemented in the solution software, as

$$\vec{f}_{M_\ell} = \varepsilon_g\rho_\ell C_M\frac{D}{Dt}\left(\vec{U}_g-\vec{U}_\ell\right) \tag{19}$$

3.1. Added mass modeling
Two added mass coefficients are used. The first one was determined by Beguin et al. [3] (see **Figure. 5.**). Beguin et al. [3] simulated random bubble clouds of different sizes and averaged its results to propose the added mass correlation for the Euler-Euler Model. All bubbles accelerated equally along the z-direction. The added mass coefficient (20) was determined for the center bubble taking into account all the surrounding bubble acceleration. Thus, this formulation includes both the added mass and the induced added mass. The added mass in the x and y direction (i.e. the perpendicular plane to the bubbles acceleration) are considered as zero based on the fitting presented in **Figure 5.**. Therefore, the added mass tensor can be reduced to a scalar since the only remaining added mass force is along the acceleration direction. Consequently, the added mass coefficient is given as follows :

$$C_M = \frac{1}{2}+0.36\varepsilon_g^2 \tag{20}$$

However, we observe in **Figure 5.** that for some bubble clouds the added mass coefficient in both x and y directions could have relatively considerable values $(-0.25, 0.25)$ depending on the asymmetry of the cloud around the bubble. A better modeling would consider the added mass as a tensor rather than a scalar. The void fraction gradient would be a way to account for the asymmetry of the bubble cloud around the central bubble. Therefore, taking into account the void fraction gradient dependency to develop a correlation for the added mass tensor would be a solution to adequately model the added mass and Meshchersky forces, and hence, bubble dispersion.

For the purpose of comparison, the upper bound of the added mass coefficient, shown in **Figure 5.**, is also used. This correlation was developed by Zuber [11] :

$$C_M = \frac{1}{2}\frac{1+2\varepsilon_g}{1-\varepsilon_g}\approx\frac{1}{2}+\frac{3}{2}\varepsilon_g \tag{21}$$

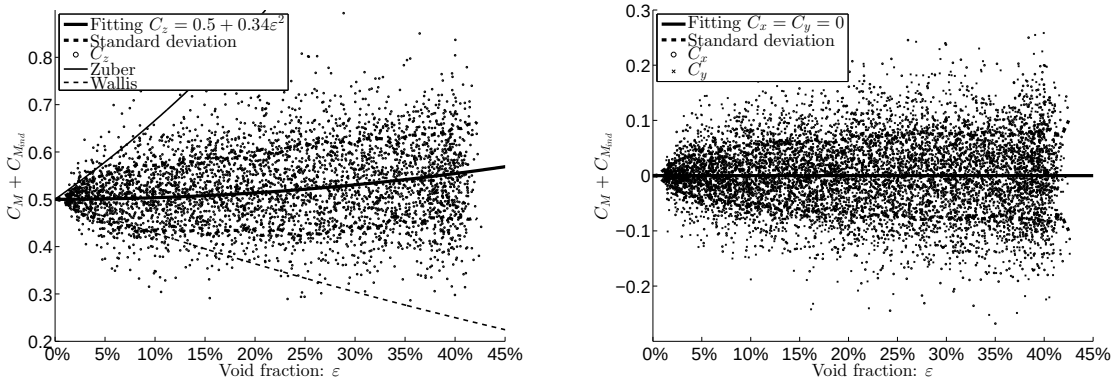

Figure 5: Values of bubble added mass for various bubble clouds generated randomly. For more details, see Beguin et al. [3].

As the added mass coefficient depends on the void fraction, we shall consider the problem as a variable mass problem. This requires rewriting the added mass force as :

$$\vec{f}_{M,\ell} = \varepsilon_g \rho_\ell \frac{D}{Dt}\left[C_M\left(\vec{U}_g - \vec{U}_\ell\right)\right] \tag{22}$$

This force can be decomposed as the classical added mass formula complemented by the Meshchersky force. Note this formula is correctly written as we consider the difference of velocity between both forces which makes it invariable by Galilean transformation.

$$\vec{f}_{M,\ell} = \underbrace{\varepsilon_g \rho_\ell C_M \frac{D}{Dt}\left(\vec{U}_g - \vec{U}_\ell\right)}_{\text{Added mass force}} + \underbrace{\varepsilon_g \rho_\ell (\vec{U}_g - \vec{U}_\ell)\frac{DC_M}{Dt}}_{\text{Meshchersky force}} \tag{23}$$

The Meshchersky force is not accounted for in the numerical solution but can be added in the form of a drag force:

$$\vec{f}_{DMe} = \frac{3}{4}\varepsilon_g \rho_\ell \frac{C_{DMe}}{d_b}\left\|\vec{U}_g - \vec{U}_\ell\right\|\left(\vec{U}_g - \vec{U}_\ell\right) \tag{24}$$

Thus, the drag coefficient stemming from the Meshchersky force can be rewritten as:

$$C_{DMe} = \frac{4}{3}\frac{d_b}{\left\|\vec{U}_g - \vec{U}_\ell\right\|}\frac{DC_M}{Dt} \tag{25}$$

Using the Beguin et al. [3] correlation :

$$C_{DMe} = \frac{4}{3}\frac{d_b}{\left\|\vec{U}_g - \vec{U}_\ell\right\|}0.72\varepsilon_g\left[\frac{\partial \varepsilon_g}{\partial t} + (\vec{U}_g - \vec{U}_\ell)\cdot\nabla\varepsilon_g\right] \tag{26}$$

Using the Zuber [11] correlation :

$$C_{DMe} = \frac{4}{3}\frac{d_b}{\left\|\vec{U}_g - \vec{U}_\ell\right\|}\frac{3}{2}\left[\frac{\partial \varepsilon_g}{\partial t} + (\vec{U}_g - \vec{U}_\ell)\cdot\nabla\varepsilon_g\right] \tag{27}$$

3.2. Drag force modeling

The drag coefficients widely used in the literature [7, 8, 12] were developed for a single spherical particle rising in a fluid. By not taking into account the surrounding bubbles, the applicability of those correlations on dispersed flows is questionable. Some correlations like [13, 14] took into account the void fraction. Those correlations were empirically obtained and their applicability range is restrained by the experimental conditions. A more general, semi-analytical solution for the drag coefficient was developed by [15]. This coefficient considers the presence of the surrounding bubbles by taking into account the effect of local void fraction :

$$C_D = \frac{16}{Re}\left[1 + \frac{2\left(\frac{2+3\bar{\mu}}{2+2\bar{\mu}}\right)^2}{1+\frac{Re_c}{Re}}\right]\frac{1-\varepsilon}{\left(1-\varepsilon^{1/3}\right)^3}\frac{P_1(\varepsilon)+\bar{\mu}P_2(\varepsilon)}{P_3(\varepsilon)+\bar{\mu}P_4(\varepsilon)} \tag{28}$$

with : $Re_c = 33 + 8600\varepsilon$
$P_1(\varepsilon) = 4 + 6\varepsilon^{5/3}$
$P_2(\varepsilon) = 6 - 6\varepsilon^{5/3}$
$P_3(\varepsilon) = 4 + 6\varepsilon^{1/3} + 6\varepsilon^{2/3} + \varepsilon$
$P_4(\varepsilon) = 4 + 3\varepsilon^{1/3} - 3\varepsilon^{2/3} - 4\varepsilon$
$\overline{\mu} = \frac{\mu_g}{\mu_l}$

3.3. Numerical approach

Numerical simulations were conducted using the commercial package $CFX19$ whose solver is based on the finite volume method. A high resolution scheme was used for advection terms ([16]). The second order backward Euler is used for time integration.
Two validation tests have been made to assess the effect of added mass on bubble dispersion which will be discussed in the following subsections: a bubble column [4] and a bubble jet in transverse flow [5]. In both cases the convergence criterium was set to 10^{-5}. The total simulation time is $T = 10s$. We compared the results for the averaged void fraction within the last $5s$ of the simulation.

3.4. Simulation of a bubble column

The bubble column used by [4] is a 3D column with a square cross section of 0.15×0.15 m^2 filled with distilled water up to a height of 0.45 m. The air was introduced into the domain by a perforated plate that contains 49 holes with 1 mm of diameter. The inlet area is 0.03×0.03 m^2 and the gas inlet velocity is $U_{g_{in}} = 0.1225$ m/s. Based on measurements in [4], the average diameter of the bubbles at the inlet is set to 4 mm. Along the walls, no-slip boundary conditions were adopted for both phases. A pressure boundary was applied at the outlet.

As shown in **Figure 6.**, a slight difference (10^{-5}) in the void fraction distribution could be seen in the edges of the bubble column using the correlation in [11]. This difference is smaller using the correlation in [3]. In fact in [3], the added mass varies weakly as a second order function of void fraction. We can conclude that for the bubble column, the Meshchersky force developed for the Euler-Euler model does not allow to capture the dispersion effect observed in the Euler-Lagrange model.

3.5. Simulation of a bubble jet in transverse flow

In [5] measurements were performed in an horizontal flume of 25 m $\times$ 1.2 m $\times$ 0.8 m. The water depth is constant and equal to 0.65 m. Since the provided images cover an area of 0.73×0.55 m^2, the numerical domain was set to those dimensions. The cross-sectional water velocity is set to 0.20 m/s. The air is injected into the system through a single nozzle with a diameter of 6 mm. The air volume flow rate at the inlet is 1 LPM which leads to a gas velocity of 1.77 m/s. The measured averaged bubble diameter is 9.84 mm.

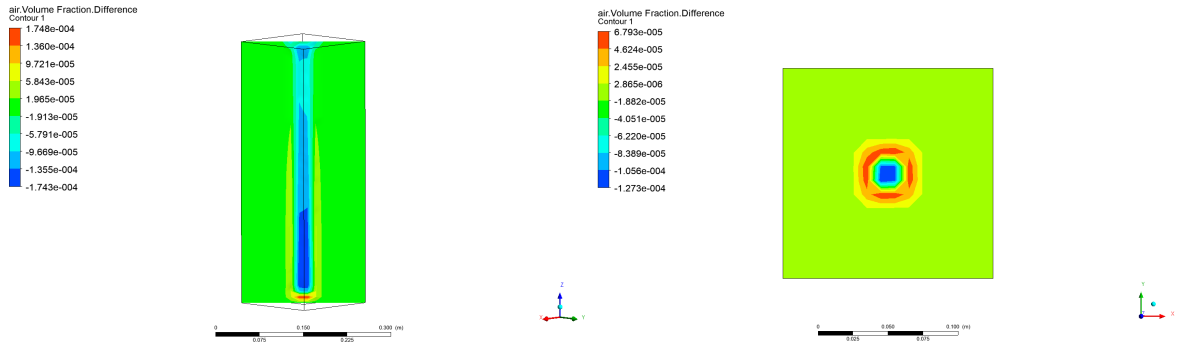

Figure 6: Difference of the Averaged void fraction distribution with $C_M(\varepsilon_g)$ (21) and $C_M = 0.5$ (up) along a transversal plane (down) along an horizontal plane at $z = 0.25$ m.

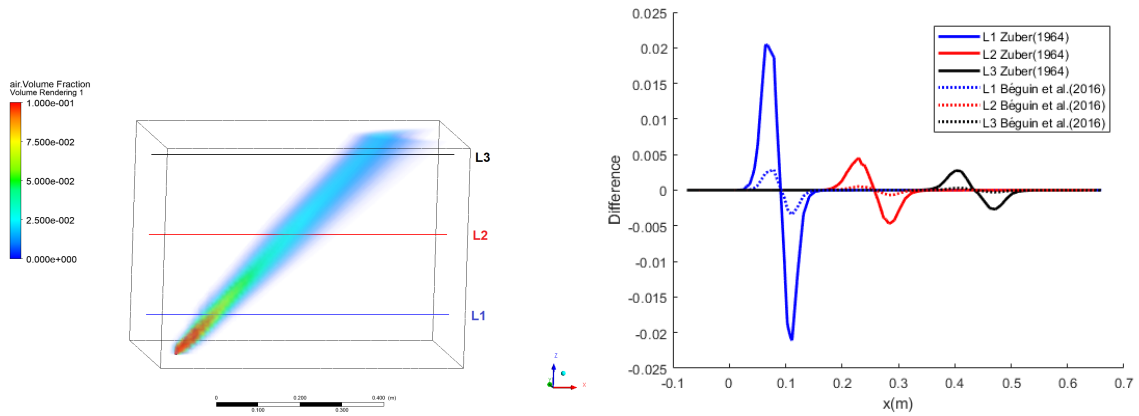

Figure 7: (Left) Numerical averaged Void Fraction in the Flume with correlation (21). (Right) Void fraction difference along horizontal lines.

The void fraction difference shown in **Figure 7.** (right) is the difference between the void fraction obtained with $C_M(\varepsilon_g)$ and $C_M = 0.5$ along the three lines shown in **Figure 7.** (left). The difference between the results obtained using the coefficient determined in [3] and a constant value coefficient is insignificant (less than 0.5%). This is due to the fact that, when averaged, added mass varies weakly as a second order function of the void fraction. For the correlation defined by Zuber [11], which is the upper bound of the added mass coefficient, the difference is around 2%. However, the only observed difference between the three cases is in the flow centerline angle. The Meshchersky force developed for the Euler-Euler model has the same form as a drag force. Including it on the numerical model modulates the drag force. Thus, the observed dispersion is in the direction of the relative velocity and it has no significant influence on the flow dispersion in the other directions. The same conclusion as for the bubble column can be drawn: the Meshchersky force developed for the Euler-Euler model does not allow to capture the dispersion effect observed in the Euler-Lagrange model.

4. Conclusion

The role of the added mass on bubble cloud dispersion was studied. We considered a more complete representation of the added mass effects that takes into account the "Meshchersky" force. This force appears naturally from potential flow pressure analysis. This part of the added mass force results from the fact that the added mass varies spatially. We thus face a variable mass problem. Two kinds of numerical simulations have been undertaken to test the effect of this more complete added mass representation

on bubble clouds. In the Euler-Lagrange approach, local effects due to bubbles arrangement on added mass are taken into account. The effect on bubble cloud dispersion was tested on simple arrangements of side-by-side bubbles. It is observed that closely packed bubble clouds expand their surface by 50% after only a few seconds. For the Euler-Euler approach, $C_M(\varepsilon)$ doesn't model local variations of the added mass due to local bubble arrangements. We observed that this prevents cloud dispersion. This is due to the fact that the Meshchersky force deduced from the Euler-Euler approach takes the form of a drag force [thus in the direction of gas-liquid velocity difference] which has almost no influence on the void fraction dispersion. The Euler-Lagrange model gave us a better understanding of the role of the added mass force on the bubble dispersion. This effect is not captured by the Euler-Euler model. In fact, based on **Figure 5.** the added mass in the plane perpendicular to the bubble cloud acceleration is zero. However, we observe for some bubble clouds the added mass coefficient in both x and y directions could have relatively considerable values $(-0.25, 0.25)$ depending on the asymmetry of the cloud around the bubble. A better modeling would consider the added mass as a tensor rather than a scalar. The void fraction gradient could be a way to account for the asymmetry of the bubble cloud around the central bubble. Therefore, future work will be to develop a correlation for the added mass tensor that takes into account the void fraction gradient dependency. This would allow to model more consistently the added mass and Meshchersky forces, and hence, allow bubble dispersion by added mass by the Euler-Euler approach.

5. Acknowledgments

This work was sponsored by the NSERC - General Electric Industrial Research Chair in two-phase flow. Their support and permission to publish this paper is gratefully acknowledged.

References

[1] Milne-Thomson L 1968 *Theorical Hydrodynamics* 5^{th} ed (New York: Macmillan)
[2] Biesheuvel A and Van Wijngaarden L 1982 *Journal of engineering Mathematics* **16** 349–365
[3] Beguin C, Pelletier E and Etienne S 2016 *Physics of fluids* **27 (12)**
[4] Deen N 2001 *An experimental and computational study of fluid dynamics in gas-liquid chemical reactors* Master's thesis Aalborg University
[5] Wenming and Zhu D Z 2013 *International Journal of Multiphase Flow* **55** 156 – 171
[6] Kumaran V and Koch D L 1993 *Physics of Fluids A: Fluid Dynamics* **5** 1123–1134
[7] Schiller L 1933 *Z. Ver. Deut. Ing.* **77** 318–326
[8] Clift R and Gauvin W 1971 *British Chemical Engineering* **16** 229
[9] Brown P P and Lawler D F 2003 *Journal of Environmental Engineering* **129** 222–231
[10] Lance M and Bataille J 1991 *Journal of Fluid Mechanics* **222** 95–118
[11] Zuber N 1964 *Chemical Engineering Science* **19** 897–917
[12] Mei R, Klausner J F and Lawrence C J 1994 *Physics of fluids* **6** 418–420
[13] Rusche H and Issa R 2000 *Japanese European Two-Phase Flow Meeting, Tshkuba, Japan*
[14] Simonnet M, Gentric C, Olmos E and Midoux N 2007 *Chemical Engineering Science* **62** 858–866
[15] Beguin C 2010 *Modélisation des écoulements diphasiques: amortissement, forces interfaciales et turbulence diphasique.* Ph.D. thesis École Polytechnique de Montréal
[16] Jasak H, Weller H and Gosman A 1999 *International journal for numerical methods in fluids* **31** 431–449